

IHTC16-23149

LOCAL AND GLOBAL HEAT TRANSFER CHARACTERISTICS INSIDE A RECTANGULAR CHANNEL OF 1:10 ASPECT-RATIO WITH RIBBED SURFACES

Alfonso Niro*1, Pasqualino Gramazio1, Luigi Vitali1, Damiano Fustinoni1

¹Politecnico di Milano, Department of Energy, Campus Bovisa, Via Lambruschini 4, 20156 Milano, Italy

ABSTRACT

In this paper we present new experimental results on both local and global heat transfer characteristics of a forced air-flow through a 12-mm-height, rectangular channel of 1:10 aspect ratio, with square-cross-section ribs mounted on the lower wall, that is also the only one heated. As local heat transfer characteristics are evaluated for fixed heat flux boundary condition whereas the global ones are for uniform wall temperature, two different test sections are used; that one for local measurements is provided with a 120 mm x 120 mm Germanium window to allow optical access inside the duct to the IR-camera. The local convective heat transfer coefficient is evaluated by accurately assessing the dispersed non-convective heat flux components. A Matlab script was specifically developed to solve the radiative heat transfer problem in a 2D cavity involving partially transparent walls and multi-wavelength regions. Moreover, much attention was also paid to evaluate the heat flux conductively diffusing through the heater plane and the walls surrounding the cavity. Data here presented refer to convection over ribs of 4-mm side in transverse configuration with a pitch-to-height ratio of 20, and for Reynolds numbers, based on the duct hydraulic diameter, ranging between 700 and 8000. Finally, the streamwise distributions of the local heat transfer coefficient are shown and compared to the flat channel.

KEY WORDS: Convection, heat transfer enhancement, heat exchanger, rectangular channel, cooling turbine blade, transverse ribs

1. INTRODUCTION

Heat transfer in forced flows through rectangular channels is encountered in a multiplicity of devices, but it is nearly never as high as desired or required; thus, ribs are an efficient and cost-effective way to improve the overall thermal performance. For this reason, forced convection inside rectangular channels with ribroughened walls, in a large variety of shape and configurations, is a subject extensively considered in literature since the 80's. Moreover, very recent publications, for instance Ruck and Arbeiter [1] and Sharma et al. [2], show that the problem of fluid-dynamic and thermal effects of rib-induced turbulence is still largely under investigation from both a numerical and experimental standpoint. Finally, during the last decade, there has been an increasing interest for channels with only one heated and ribbed surface too, as they are utilized in solar air heaters. For the latter application, Saxena et al. [3] presented a considerable literature overview on the effect of rib-enhanced channels.

The knowledge of the global heat transfer coefficient is essential to properly design channels with ribroughened surfaces, but knowing local thermal characteristics is a powerful tool in guiding the optimization of rib geometry and configuration, especially if it is possible to evaluate the full-field distribution of convective heat transfer coefficient by means of a non-intrusive measurement of the surface temperature, e.g., by thermography. Experimental measurements of local heat transfer characteristics have been carried out with various techniques by several investigators, for instance Han and Park [4], Tanda and Cavallero [5],

*Corresponding Author: alfonso.niro@polimi.it

and Wang and Sunden [6]. However, all these studies are for Re larger than 10000, whereas for lower values this kind of measurement poses interesting issues, mainly for the unavoidable problem of accurately assessing each contribution of the several and simultaneous heat transfer processes, as their overall percentage weight increases as Re decreases, till reaching 50% at Re=2200.

The ThermALab laboratory of the Energy Department at Politecnico di Milano has been investigating forced convection inside ribbed rectangular channels for many years. Studies have been carried out by experimentally analysing the global thermal performance and the pressure-drop induced by a large variety of rib configurations, as well as local heat transfer characteristics by means of IR thermography [7] and, previously, of holographic interferometry and background oriented Schlieren (BOS) techniques. Furthermore, newly DNS studies are also being carried out to integrate the experimental observations. In the context of this project, the experimental apparatus has been lately re-designed [8], in order to minimize thermal dispersions, and all the procedures to evaluate heat transfer coefficient distribution from full-field surface temperature measurements by IR-thermography have been critically assessed [9]; further improvements are also presented in this paper. In particular, the new adopted procedures allow to evaluate heat transfer coefficient even close to the channel sides, where it is overlooked to our best knowledge of open literature.

2. EXPERIMENTAL SET-UP

The measurements have been carried out on an open-loop channel operated in suction with two different test sections, but with the same dimensions as summarized in table 1, because of the diverse thermal boundary conditions imposed on the channel lower wall when the global heat transfer characteristics and the local ones are analysed. The former, indeed, is for uniform temperature whereas the latter for fixed heat flux. The test section used in the first case is described in detail in [8], whereas the other in [9] but it is also schematically shown in figure 1. Summarizing its main features, the channel lower surface is heated by means of two Printed Circuit Boards (PCBs) independently powered and controlled. The PCBs have a substrate made of FR-4 fiberglass-reinforced epoxy laminate material, whereas copper tracks are 0.017 mm thick, 7.8 mm wide, spaced 0.2 mm apart each other, and covered by a black lacquer which also fills up the gaps between them, making the heating surface perfectly flat, smooth and with a high emissivity. A Hendress Hauser T-Mass 65F15 flow meter is used for automatic mass-flow rate readings. A double-glazing 130 mm x 130 mm germanium window grants the optical access to a FLIR T650sc IR-camera, with a 640 x 480-pixel resolution.

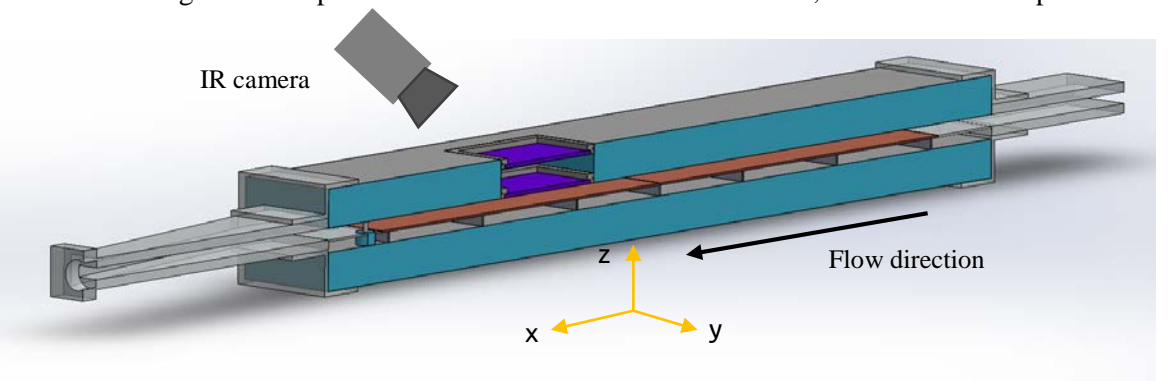


Fig. 1 Section of the test channel for local heat transfer measurements, with constant heat flux

Punctual temperature measurements are also carried out for reference by RTDs and thermocouples, as reported in table 2. The remaining temperatures, whose knowledge is needed to determine the convective heat flux distribution, are evaluated on the basis of the following assumptions summarized in table 2 as well: air bulk temperature $T_b(x)$, whose measurement is accurately described in [8], increases linearly along the test section from the inlet value to the outlet one, as supposed by reference works [4]; the temperature of the germanium window $T_{ger}(x,y)$ is uniform and equal to temperature T_{up} measured on its frame, as its conductivity is two orders of magnitude higher than all the other parts of the channel (this assumption is also

supported by a sensitivity analysis performed with a numerical model of radiative heat exchanges and it is discussed in the section 3.6). Finally, the channel side wall temperature $T_{side}(x,z)$ is assumed to be constant along z-direction and equal to the mean between T_{up} and the breadboard temperature T_{down} measured at the channel side.

Table 1. Main experimental features

h	Channel height	12	mm
\boldsymbol{L}	Channel length	840	mm
w	Channel width	120	mm
D_h	Hydraulic diameter	21.82	mm
h/w	Height to width ratio	0.10	
S	Rib side dimension	4	mm
d	rib-to-rib distance	80	mm
A_s	Total heated surface	0.1	m^2
Re	Reynolds number	700 = 8000	

Table 2. Main measured and derived temperature values

Measured Temperature	Symbol	Probe kind/Instrument
Bottom wall surface	$T_w(x,y)$	IR camera
External (ambient)	T_{ext}	PT100 RTD
Inlet air bulk temperature	T_{in}	PT100 RTD
Outlet air bulk temperature	T_{out}	PT100 RTD
Channel upper side wall	T_{up}	T-type thermocouple
Derived Temperature	Symbol	Method
Bulk temperature	$T_b(x)$	Linear interpolation between T_{in} and T_{out}
Channel side wall	$T_{side}(x,z)$	Mean between T_{up} and $T_w(x, w/2)$
Germanium window surface	$T_{ger}(x,y)$	Uniform and equal to T_{up}

3. METHODS AND PROCEDURES

3.1 Global heat transfer coefficient The global heat transfer coefficient $h_{glob,T}$ and the related Nusselt number $Nu_{glob,T}$, for uniform channel wall temperature, are evaluated as

$$h_{glob,T} = \frac{\dot{Q}/A_{S}}{\Delta T_{m,Log}} = \frac{\dot{m}c_{p,air}(\theta_{i} - \theta_{o})}{A_{S}[(\theta_{i} - \theta_{o})/\ln(\theta_{i} / \theta_{o})]} = \frac{\dot{m}c_{p,air}}{A_{S}} \ln \frac{\theta_{i}}{\theta_{o}}$$
(1)

$$Nu_{glob,T} = \frac{h_{glob,T}D_h}{k_{air}} \tag{2}$$

where \dot{Q} the total exchanged heat power; A_S and D_h the total heated area and the hydraulic diameter, respectively, as reported in table 1; θ_i and θ_o the wall-to-air-bulk-temperature differences at the entrance and exit, respectively, of the test section; \dot{m} the air mass-flow-rate. Finally, for our purposes, air thermo-physical properties, namely, specific heat at constant pressure $c_{p,air}$ and thermal conductivity k_{air} , are supposed to be independent of temperature along the test section. The analysis performed according to Moffat [11] gives an uncertainty on the global convective coefficient at most equal to 5%. The local results, even though measured with a constant heat flux boundary condition, are compared to the global ones in paragraph 4.1 by averaging them on the rib-to-rib measured region, thus obtaining $h_{ave,q}$ and the related Nusselt number $Nu_{ave,q}$.

3.2 Local convective heat transfer coefficient The local convective heat transfer coefficient $h_{loc,q}$ and the related Nusselt number $Nu_{loc,q}$ are evaluated, for the channel with constant heat flux, as

$$h_{loc,q}(x,y) = \frac{q_c''(x,y)}{T_w(x,y) - T_b(x)}$$
(3)

$$Nu_{loc,q}(x,y) = \frac{h_{loc}(x,y)D_h}{k_{air}}$$
(4)

where $q''_c(x,y)$ and $T_w(x,y)$ the punctual values of convective heat flux and surface temperature, respectively, and $T_b(x)$ the air bulk temperature. It was already reported about T_b whereas the measurement of T_w , by means of IR-thermography, is described in detail in section 3.5, hence the only term which requires a further specification is $q_c(x,y)$. It is obtained by a steady-state balance on the copper track layer, schematically shown in figure 2, assuming no temperature variation across its thickness being the layer very thin

$$q_c''(x,y) = \sigma_{el} s_{Cu} - q_r''(x,y) - q_{kz}''(x,y) + q_{kxy}''(x,y)$$
 (5)

where σ_{el} the volumetric heat dissipation due to the Joule effect, considering a uniform generation, s_{cu} the layer thickness, $q''_{r}(x,y)$ the heat flux radiated by the layer coating, $q''_{kz}(x,y)$ the heat flux diffusing in z direction from the rear of the copper track layer toward the substrate inside, and finally $q''_{kzy}(x,y)$ the heat flux diffusing in x-y direction through the layer itself. In particular, in streamwise x direction that is parallel to the copper tracks, it is considered negligible due to the small values of temperature gradient in that direction; in spanwise y direction, it is calculated for each \bar{x} , assuming a fictitious homogeneous material, as

$$q_{kxy}^{"}(\bar{x},y) = k_{eq} s_{Cu} \left(\frac{\partial^2 T_w}{\partial y^2} \right)$$
 (6)

where k_{eq} the equivalent thermal conductivity, resulting from the series of the copper tracks and the lacquer filling the gaps between them, as schematically shown in figure 2. Both $q''_{kz}(x,y)$ and $q''_{r}(x,y)$ are calculated by means of two distinct models presented in the next two sections. The solution strategy is to apply those models on N_x independent 2D y-z slices of the test section, instead of solving two 3D problems, in order to reduce computational times and complexity without losing accuracy, as discussed at the end of the section 3.6.

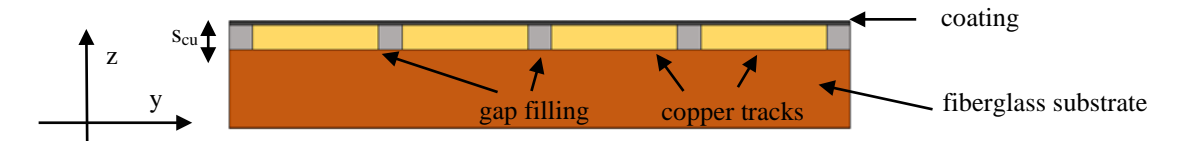


Fig. 2 PCB scheme in x-y direction

3.3 FEM model of the test-section A 2D FEM thermal model of the test apparatus in a y-z cross-section has been developed in COMSOLTM, featuring the following components: PCB (only substrate), PMMA frames, germanium double window, extruded-polystyrene (XPS) insulating walls, and the two layers of still air, namely, between the two germanium windows, and underlying the PCB. The model is purely conductive even within the air layers but verifying a-posteriori that free convection cannot occur. A free-convection boundary condition is assumed for the external walls of the test-apparatus, whereas temperatures are assigned over the test-section inner walls. Indeed, the temperatures of the side and upper walls of the channel are T_{side} and T_{ger} , respectively, and are evaluated as discussed above. The temperature distribution over the substrate upper surface is exactly the same as that measured over the coating, i.e., $T_w(x,y)$, because it was assumed that temperature variations across the copper track layer are negligible as well as its contact thermal resistance with the substrate. The solution of the model allows to evaluate, at any given section \bar{x} , the spanwise distribution of the heat flux $q''_{kz}(\bar{x},y)$ diffusing in z direction from the upper surface of the substrate toward its inside, that appears in equation 5.

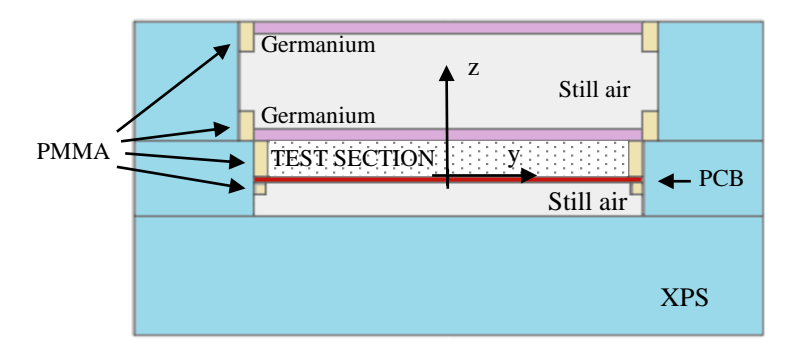


Fig. 3 Geometry of the 2D FEM model of conductive heat transfer in the channel cross-section

- **3.4 Radiative heat flux model** A 2D radiative heat transfer model was developed in [9] to precisely evaluate, for each given \bar{x} , the spanwise distribution of heat flux $q''(\bar{x},y)$ radiated by the copper track coating, from the temperature distribution $T_w(x,y)$ measured over it. The equation set is based on a slight modified version of Siegel's model [12], which describes the radiative heat transfer for cavities composed by semi-transparent, diffuse and selective surfaces. The spectral behavior is considered by solving the problem for three wavelength regions, i.e., between 0 and 7 µm, 7 and 13 µm, and from 13 µm up, which are determined by the selective behavior of the germanium window. The optical properties have been measured by means of MIR spectrometry up to 20 µm at the ThermALab, as also reported in [9].
- **3.5** Analysis procedure All measurements and models described in the previous sections are combined to retrieve the local heat transfer coefficient distribution. The experimental procedure starts by imposing the electrical power input \dot{Q} and the air mass flow rate \dot{m} . When the steady state condition is attained, and this is supposed to occur when local temperature time-fluctuations are contained in a band of 0.02 K, a sequence of 30 thermograms is acquired in 1 s as well as data from all thermocouples and RTDs are collected. The sequence is then time-averaged pixel-by-pixel so to obtain just one IR-thermographic image with a lower white noise. Temperature values are retrieved from thermograms by means of a custom calibration performed on a body, with the same surface finish as the heater, kept at fixed and uniform temperature, and through the same optical setup and view angle used on the channel. The temperature field is furtherly elaborated; in particular, it undergoes first an inverse projection transform, to recover an undistorted view, and then an additional filtering, namely, by interpolating data in the sense of least squares versus spatial coordinates x-y with a polynomial, in order to eliminate spatial high frequency disturbances and to grant a proper differentiability. As final result, a matrix with the temperature map of the channel lower wall surface $T_w(x,y)$ is obtained. Next, using in a given section \bar{x} this map together with the temperatures of the other channel walls, i.e., $T_{side}(\bar{x},z)$ and $T_{ger}(\bar{x},y)$, the heat flux distributions $q''_{kz}(\bar{x},y)$ and $q''_{r}(\bar{x},y)$ are evaluated as described. This evaluation is repeated for 50 values of \bar{x} , i.e., 50 y-z slices of the test section. Eventually, $h_{loc,q}(x,y)$ and $Nu_{loc,q}(x,y)$ are evaluated by equations 3, 4, and 5. This process is carried out for seven values of Reynolds numbers ranging between 700 and 7550.
- **3.6 Uncertainty analysis** The adopted analysis procedure involves, as just described, experimental measurements as well as procedural and modeling choices; hence the uncertainty sources associated with each of them have been carefully considered and taken into account for an overall error estimate. Measurement uncertainties are due to temperature sensors, IR-camera, and mass-flow-rate meter. As stated in [8], the standard deviation of thermocouples and thermo-resistances has been evaluated by a calibration procedure in a temperature-controlled water bath, resulting in 0.02 K and 0.01 K respectively. The declared NETD of the IR camera, i.e. 0.02 K at 300 K, has been also verified in the entire measurement range. The mass-flow-rate meter has been calibrated by the Italian "Istituto Nazionale di Ricerca Metrologica (INRiM)", and a 2 % accuracy is proven for the range of Reynolds numbers exploited in this research.

The procedural uncertainties are mainly caused by the spatial filtering of the temperature field measured over the heated surface. To reduce this source, the degree of the interpolating polynomial has been chosen thus to minimize the value of R^2 that, eventually, turns to be 0.98 [8].

Uncertainties from the FEM model of test-section (section 3.3) arise from several factors, namely, the correctness of thermophysical property values, the accuracy of evaluation of thermal dispersion by free convection from the test-apparatus external walls, and the modeling choices with particular concern to the effects on the solution of assuming a uniform temperature along the channel inner side walls, as well as of the unknown value of the contact thermal resistance between breadboard and its supporting structure. Thermal conductivities of all test-section materials have been measured in the ThermaLab laboratory with an uncertainty at most of ± 4 %; heat transfer by free convection is significantly lower than the other thermal transport phenomena and, hence, practically unable to alter local heat flux distribution on the breadboard surface. Finally, the effects of the two considered modeling choices have been assessed by comparing the values of q''_c calculated with our assumptions with those obtained while varying the thermal contact resistance values and the temperature distribution on the side walls. The outcome is that this modeling error, as shown in figure 4, is practically null up to a distance y from the section center-line of 40 mm, next it starts to slowly increase, yet remaining below 10% as far as y=56.5 mm, and after that it is quickly diverging.

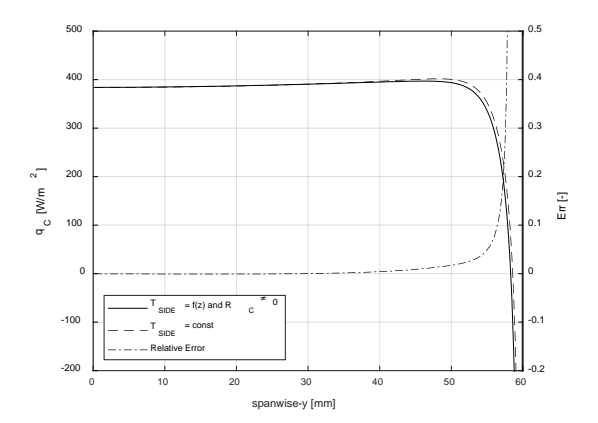


Fig. 4 Spanwise convective heat flux, for uniform and variable temperature of the side wall, and relative error between them

Finally, uncertainties from the radiative model (section 3.4) are due to the radiative properties, surface discretization, and 3D effects given by radiative heat transfer toward channel surfaces upstream and downstream the considered y-z slice. Radiative properties have been measured with an uncertainty of ± 1 % up to 20 μ m, and a constant behavior is assumed after that wavelength. Surface discretization error is minimized by a sensitivity analysis; 3D effects have been found to be negligible by comparing the 2D results to a full 3D model.

Considering all the aforementioned sources of uncertainty, the uncertainty on the measurement of $h_{loc,q}(x,y)$ is estimated to be $\pm 7\%$; however, a full evaluation by Monte-Carlo methods is planned.

4. RESULTS

4.1 Global The average rib-to-rib Nusselt $Nu_{ave,q}$ in this experimental set-up have been calculated to test the consistency of the results with the global ones at constant temperature, and the results are shown in figure 5. In the flat channel case, the agreement with the trend of the correlations by Shah and London for Re<2300 and by Gnielinsky for higher Re is good in both cases. The Nu increase given by the ribs is also shown, as well as the absence of a definite transitioning point, as the ribs acts as turbulence triggers. The differences between the two set-ups, which are between 10% and 17%, are reduced to less than the experimental uncertainty if Hausen's correction is taken into account. Finally, for Re=700, Nu for the ribbed and flat channel are close.

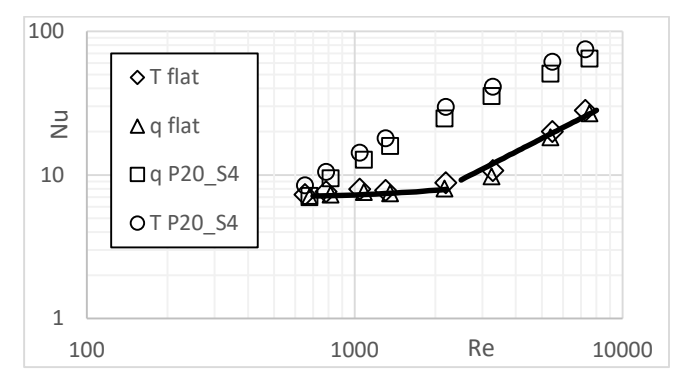


Fig. 5 Nusselt number vs Reynolds number for flat channel (flat) and for transverse ribs (P20_S4), global values with uniform wall temperature (T) and averaged local with fixed heat flux (q)

4.2 Local The local results show interesting trends. In detail, figure 6 shows the contour plots of $Nu_{loc,q}(x,y)$ of a rib-to-rib section of the channel, for the minimum, an intermediate and the maximum tested Re, i.e. Re=700 (a), Re=5400 (b) Re=7550 (c). It can be noted that for Re=700 the rib has no relevant effect on the distribution of Nu; in fact, streamwise variations are negligible, as expected for the laminar flow regime. For higher Re, the Nu distribution shows a peculiar behavior, which is characterized by both the well-known peak at the reattachment point in the streamwise direction, and by a peculiar increase towards the lateral walls before a sudden drop, which is likely due to secondary flows first observed by Nikuradse [13] and further investigated by Gavrilakis [14].

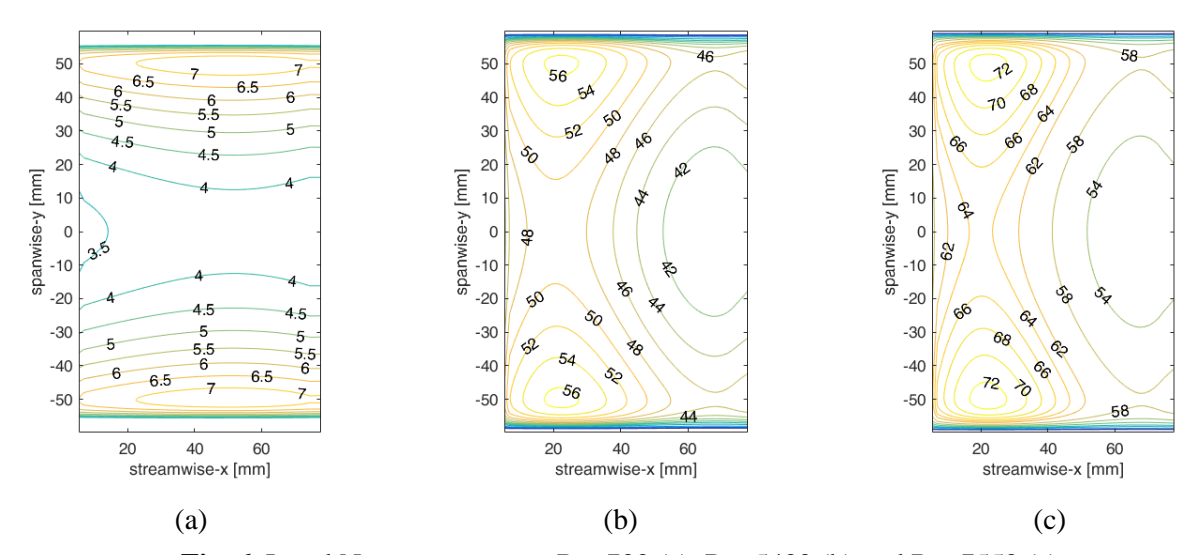
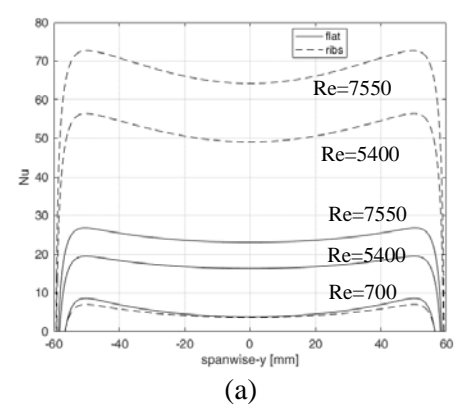


Fig. 6 Local Nu contour maps, Re=700 (a), Re=5400 (b) and Re=7550 (c)

Figure 6 (a) highlights the spanwise trend of Nu_{loc,q} for x=20 mm, which is the local streamwise maximum for the ribbed configuration, showing its rise towards the edges both for the flat and the ribbed channel, again for the minimum, maximum, and intermediate Re. This rise is 12% with respect to the center value for the ribbed channel, and 14% for the flat channel, and the peak lies at y=±50 mm. Since the possible modeling error in that point is below 2%, as it can be seen from figure 4, and the experimental uncertainty is below 7%, this rise close to the wall, though probably with a lower extend than that shown in figure, seems actually due to the aforementioned fluid-dynamics effects, both for the ribbed and flat channel. It is also interesting to analyze the streamwise Nu increments for the ribbed configuration with respect to the flat channel, i.e., Nu/Nu₀. Figure 7 (b) shows the streamwise trend for all the tested Re, and it can be seen that there is little to no increment for Re=700, then an increasing increment up to Re=2200, after which, for higher Re, the peak increase settles between 3.4 and 3.7. This trend is coherent with figure 5, for the global Nu.



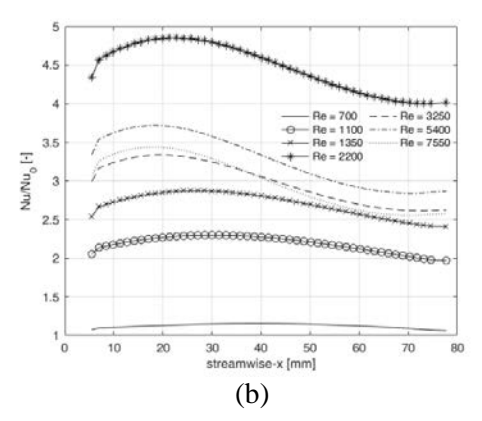


Fig. 7 Spanwise local Nu trend at x=20 mm for min, max and intermediate Re (a); streamwise Nu increment with respect to the flat channel for each tested Re

5. CONCLUSIONS

The present study shows an in-depth assessment of a coupled experimental-numerical procedure for the measurement of the local heat transfer coefficient in a rectangular channel, as well as the results for transverse ribs. All the possible sources of errors have been evaluated in the procedure, however, the lack of knowledge of the contact thermal resistance between the heater and the channel structure can lead to significant errors close to the edges, where the conductive heat flux is relevant. This uncertainty can be solved by possible modifications of the experimental apparatus to minimize it, or measurements to determine it. The peculiar humpy behavior of the spanwise convective heat transfer coefficient, i.e., its rise towards the edges before the sudden drop, is larger than the experimental uncertainty and it peaks before the rise of the modeling uncertainty, therefore it is considered to be due to the fluid-dynamics effects of secondary flows. Work is going on analyzing other rib configurations, while flow visualization and DNS analysis being in progress to get insight into fluid dynamics, especially in the proximity of the walls.

REFERENCES

- [1] Ruck, S., Arbeiter, F., "Detached Eddy simulation of turbulent flow and heat transfer in cooling channels roughened by variously shaped ribs on one wall" *Int. J. of Heat and Mass Trans.*, 118, pp. 338-401 (2018).
- [2] Sharma, N., Tariq, A., Mishra, M., "Experimental investigation of flow structure due to truncated prismatic rib turbulators using particle image velocimetry" *Exp. Therm. and Fluid Sci.*, 91, pp. 479-508 (2018).
- [3] Saxena, A., Varun, El-Sebaii, A.A., "A thermodynamic review of solar air heaters," *Ren. and Sust. En. Rev.*, 43, pp. 863-890 (2015).
- [4] Han, J. C., Park, J. S., "Developing heat transfer in rectangular channels with rib turbulators" *Int. J. Heat and Mass Trans.*, 31, pp. 183-195 (1988).
- [5] Tanda, G., Cavallero, D., "Heat transfer coefficient measurements in ribbed channels using liquid crystal thermography" *Proc. of 10th Int. Symp. on Flow Vis.*, F0038 (2002).
- [6] Wang, L., Sundén, B., "Experimental investigation of local heat transfer in a square duct with continuous and truncated ribs" *Exp. Heat Trans.*, 18, pp. 179-197 (2005).
- [7] Fustinoni, D., Gramazio, P., Colombo, L.P.M., Niro, A., "First average and local heat transfer measurements on a forced airflow at low Re-numbers through a rectangular channel with ribbed surfaces" *J. Phys.: Conf. Ser.*, 395 012042, (2012).
- [8] Fustinoni, D., Gramazio, P., Vitali, L., Niro, A., "New experimental results on local heat transfer inside a rectangular channel with rib-roughened surfaces" *J. Phys.: Conf. Ser.*, 796 012015, (2017).
- [9] Gramazio, P., Vitali, L., Fustinoni, D., and Niro, A., "New data processing of local heat transfer coefficient inside a rectangular channel" *J. Phys.: Conf. Ser.* 923, 012052 (2017).
- [10] Fustinoni, D., Gramazio, P., Colombo, L.P.M., Niro, A., "Heat transfer characteristics in forced convection through a rectangular channel with broken V-shaped rib roughened surface" *J. Phys.: Conf. Ser.*, 655 012060, (2015).
- [11] Moffat, R.J., "Describing the uncertainties in experimental results" Exp. Therm. and Fluid Sci., 1, pp. 3-17 (1988).
- [12] Siegel, R., "Net Radiation Method for Enclosure Systems Involving Partially Transparent Walls" NASA note D-7384 (1973).
- [13] Nikuradse, J., "Untersuchungen über die Geschwindigkeitsverteilung in turbulenten Strömungen" *VDI-Forschungsheft*, 281 (1926).
- [14] Gavrilakis, S., "Numerical simulation of low-Reynolds-number turbulent flow through a straight square duct" *J. Fluid Mech.*, 244, pp. 101-129 (1992).